Journal Name

Dynamic Article Links ►

Cite this: DOI: 10.1039/c0xx00000x

www.rsc.org/xxxxxx

ARTICLE TYPE

Ion adsorption on the Inner surface of Single-walled Carbon Nanotubes used as Electrodes for Electric Double-Layer Capacitors

Ayar Al-zubaidi,[a] Tsuyoshi Inoue,[a] Tomohiro Matsushita,[a] Yosuke Ishii[a] and Shinji Kawasaki *[a]

Received

DOI:

In the present study, ion adsorption on the outer and inner surfaces of single-walled carbon nanotubes (SWCNT) in different aqueous and organic electrolytes was analysed. It was found that the fundamental properties of tube size and electronic structure, particularly the transition between van Hove singularities (the band gap), reflected by the shape of the cyclic voltammogram and increase in the number of charge carriers upon doping, and apparently provided additional energy for ion adsorption inside open-end SWCNTs. In addition, when cyclic voltammogram recorded at different potential scan rates were observed, the outer surface of the tubes demonstrated the behaviour of a flat electrode with less dependence on the potential scan rate when compared to the inner surface, which acts as a porous electrode showing an ohmic drop and a distorted voltammogram at high scan rates. Mathematical analysis showed that opening the inner channel of the tubes increases electrode resistance, and that the magnitude of variation in the resistance depends on the type of electrolyte.

1. Introduction

Low energy density, is one of the major disadvantages of the electric double-layer capacitor (EDLC), and has been the focus of many research efforts over the past few decades. Increasing the energy output of EDLCs is essential for their use in electrical vehicles as high power, next generation replacements for rechargeable batteries.

EDLCs rely on a physical storage mechanism in which ions of an electrolyte are reversibly adsorbed onto a porous electrode.[1] Therefore; high energy storage in EDLCs necessitates the development of an electrode material that exhibits high electrochemical and temperature stability, as well as high accessibility for the electrolyte ions. Maximization of ion accessibility can be accomplished either by increasing the material surface area or by designing the pore structure of the electrode material for optimum electrolyte uptake. The effectiveness of the first approach is limited, which is similar to the case of activated carbon. Activated carbon, which has a high surface area compared to other materials, is most commonly used in commercial EDLCs. It has exhibited a reduction in both stability and conductivity with increasing surface area.[2] The second approach requires precise knowledge of the specific ion-pore size relationship. Materials with well-defined and controllable pore structure have proved to be promising not only for energy storage but also in terms of utilizing their predefined structure to identify the precise ion adsorption behaviour in relation to the pore structure.[3-11]

Such optimization requires detailed knowledge of the composition of the ionic layer close to the polarized electrode surface. A pore size comparable to that of the ion was shown experimentally and theoretically to cause an anomalous increase in the capacitance suggesting that the arrangement of ions near charged surfaces does not universally follow the classical Helmholtz interpretation;[5,9,13] rather depends on the length scale of the porous structure. The anomalous increase in capacitance in nanoporous electrodes was analytically addressed in terms of the reduction of the electrostatic interaction between adsorbed ions leading to close packing of the ions inside those pores creating the so called "superionic" state [13, 14] hence a separate model known as the electrical wire in cylinder capacitor EWCC was proposed to describe the adsorption of ions in nanopores.[15] It follows that the several factors of relevance to the formation of the double layer will interact to give the final value of electrode capacitance, which necessitates a combined analysis of the pore size, shape, distribution, influence of ion solvation shell and applied potential required to maximize the energy storage, as has been recently shown for slit-shaped model pores of different size distribution under different applied potentials.[16]

As energy storage electrode material, single-walled carbon nanotubes (SWCNT) have low electrical resistivity that allows fast electron transfer, and a unique nanoscale, controllable tubular morphology promising with superior ion accessibility in contrast to activated carbon whose intrinsically random and extremely complicated porous structure imposes a limitation on both the ion transfer inside the pores and the possibility of controlling the structure. SWCNTs offer moderate surface area that can be increased either by growing the nanotubes as vertically aligned forests[17] or by creating windows on their walls to utilize their inner surfaces as ion adsorption sites.[18] In terms of ion adsorption SWCNTs potentially have three adsorption sites, the outer surface of the tube/bundle of tubes, the interstitial space between

tubes, and the space inside the tubes. Several previous experiments that investigated lithium intercalation, or methane and fullerenes filling into SWCNTs, have demonstrated an increase in the amount of the stored species upon etching or creating defects, which might provide the diffusing species additional access inside the tubes.[19] However, the potential advantage of the space inside SWCNTs is not limited to providing additional storage; this internal space predictably provides superior confinement properties. The nano-size induced capillary action leads to absorption of dipolar molecules and efficient filling of SWCNTs.[20] Also, the confinement of material a within the nanoscale space in carbon nanotubes has been reported to induce peculiar physical phenomena that are different from those in the bulk phase; for example, the quasi-high pressure effect had diverse effects on the confined material, [21, 22] such as super compression resulting in a high-pressure phase structure.

It is important to define where and how the double layer is formed in a polarized SWCNT electrode, and the characteristics of the capacitance obtained from each potential adsorption site. In addition, the electrochemical behaviour of SWCNTs is also influenced by their electronic structure. Due to the unique one-dimensional electronic density of states of SWCNTs, the variation in their charge carrier density and electrode capacitance is expected to be conspicuous and sharply defined in relation to the cell applied potential. However, this is not observed in most of the previous studies for reasons, such as low purity and crystallinity and wide diameter distribution of the samples.[18, 23–30] therefore, the unique electronic density of states of SWCNTs that signals the energy required to increase the charge carrier density and increase the electrode capacitance should also be defined included as a design factor directly related to the tube size.

In a previous study, [31] we reported that opening SWCNT caps led to an increase in the total electrode capacitance and a noticeable change in the manner of ion adsorption, which was evident from the deformation of the cyclic voltammogram of open-end SWCNT electrodes at high potential scan rates. In contrast, the closed-end tubes maintained a uniform shape on the voltammogram despite the increased potential scan rates. This suggested that decapping SWCNTs introduced a surface structure that changed the ion adsorption behaviour of SWCNTs. In addition, as the applied potential was increased, a sudden, sharp increase in the electrode capacitance was observed, which was represented by “dumbbell-like” shape of the cyclic voltammogram unlike previously observed. To identify the origin of these two issues, the present study investigates ion storage and electrochemical behaviour in both closed-end and open-end SWCNTs of different sizes, in different electrolyte solutions, and under different potential scan rates. The results show a characteristic size-dependent cyclic voltammogram of SWCNTs of different diameters and a fundamental difference in ion adsorption and electrochemical behaviour between the outer and inner surfaces of SWCNTs.

2. Results and discussions

The Raman spectra of the SWCNTs samples used in this study are shown in Figure 1. The spectra show that the two investigated SWCNTs samples are well crystallized and have few defects on their surface structure, which is evident from the intensity of the D-band for both samples. The difference between the two samples in terms of frequency range of the radial breathing mode (RBM) band reflects the difference in the diameters of the samples. The narrow diameter distribution in the samples is indicated by the narrow range of the RBM band, as shown in Figure 1.[32]

However, because Raman spectroscopy is a resonance influenced process, an accurate calculation of the mean tube diameter is not possible; a more reliable technique is needed for this purpose. Consequently, the mean tube diameter for both samples was determined by simulating the experimentally observed X-ray diffraction (XRD) results, as shown in Figures S1 and S2. The detailed simulation procedure has been reported in a previous report.[31] The obtained mean diameters of 1.48 and 1.36 nm were assigned to samples A and B, respectively.

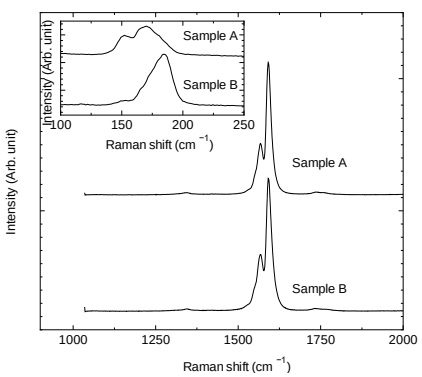

Fig.1 Raman spectra of closed-end SWCNTs of samples A and B

The cyclic voltammograms for the two samples in $TEMABF_4$/PC lead to three observations, all of which are evident in Figure 2. The first is that the unusual dumbbell shape previously discussed [31] is seen for both samples A and B. Both voltammograms presented in Figure 2 resemble a dumbbell with a “dumbbell grip” shaped region near the open circuit voltage followed by an abrupt increase in the capacitance, resulting in two step-like humps on both sides of the voltammogram.

Cite this: DOI: 10.1039/c0xx00000x

www.rsc.org/xxxxxx

ARTICLE TYPE

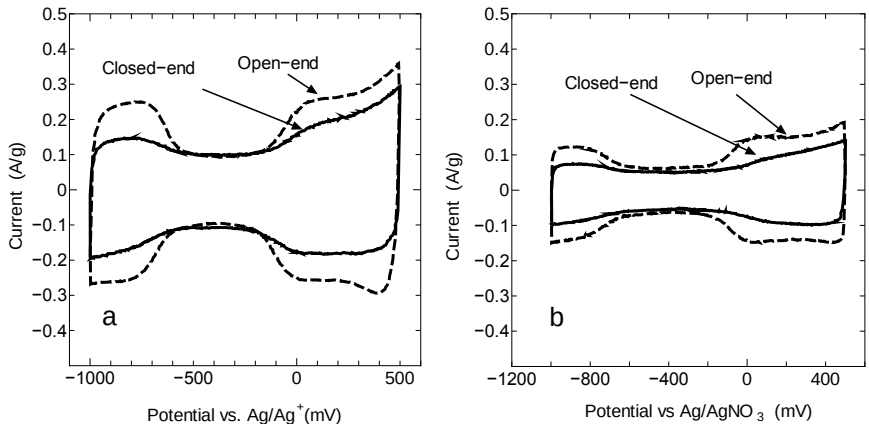

Fig.2 Cyclic Voltammograms of SWCNTs in TEMABF$_4$/PC (a) sample A (b) sample B

The second important observation is that there is a difference between sample A and sample B in terms of the width of the dumbbell "grip distance." The third observation is that, for both samples A and B, the height of the dumbbell hump (obtained electrode capacitance) of the open-end tubes is greater than that of the closed-end tubes. It must be noted that the first two observations concerning the shape of the cyclic voltammogram have been discerned in two different, well crystallized SWCNT samples.[33] Thus; the dumbbell voltammogram reflects a characteristic feature resulting from the intrinsic nature of SWCNTs. To understand this feature, the characteristic electronic density of the states of samples A and B must be assessed. To achieve this, we used the representative average diameters calculated from XRD simulations to assign approximate representative chiralities to the two samples. We have assigned (15, 6) metallic and (17, 3) semiconducting SWCNTs as representative chiralities for sample A; (14, 5) metallic and (16, 2) semiconducting SWCNTs were chosen to represent sample B.[34] This previously discussed approach[31] is justified by the fact that the two samples exhibit a limited number of chiralities owing to narrow diameter distribution. The existence of other chiralities will not introduce any significant variation in the value of the band gap or electronic density of states of the chosen representative chiralities, (17, 3) and (16, 2).

By examining the two cyclic voltammograms in Figure 2, it was found that the approximate "grip distance" of sample A was 565 mV, while that of sample B was 640 mV. A comparison of these two values with the Kataura plot (Figure S3) shows that similar differences between the band gap energies of the two representative chiralities can be obtained.

Figure 2 supports the third observation. The values of electrode capacitance of samples A and B in the dumbbell "hump" region show that open-end SWCNTs have higher capacitance than closed-end SWCNTs. This apparently occurs in the post-doping stage after the applied potential reaches the value that initiates carrier doping, which suggests that increase in the number of charge carriers is provides sufficient additional energy to push the ions inside the decapped tubes, and this additional ion adsorption could have increased the obtained capacitance.

Nevertheless, we must address the possibility that other factors caused the additional capacitance in open-end tubes, for example, functional groups or defects that may have resulted from the decapping treatment. The Raman spectra of the decapped samples (Figure S4) show that the intensity of the D-band for samples A and B has been maintained, which indicates that tube decapping could not have caused variation in the level of defects could. Also, the N_2 adsorption measurement (Figure S5 and S6) shows that the SBET of the decapped tubes is significantly higher than that of closed end tubes (values listed in Table S1). Therefore, open-end tubes definitely had more space for possible additional ion adsorption. More importantly, it should be noted that reduction-oxidation reactions manifest on the cyclic voltammogram in the form of two peaks symmetrically located around the open circuit voltage. The separation distance and height of these peaks are functions of the characteristics of the electrolyte. They may vary or disappear depending on the type of the electrolyte used. The shape of the humps in Figure 2 suggest that the peaks are located at the same values of the applied potential, and thus, peak separation and symmetry are absent around the open circuit voltage. It is also evident that instead of being sharp, the peaks are "stepped." To confirm the hypothesis about the identity of the dumbbell humps, the same samples must be tested in different electrolytes under potential window that extends to about 350 mV to each side of the center of the dumbbell grip (a total potential window of 700 mV). This potential window should be large enough to achieve an energy transition between two symmetric VHSs that are separated by a band gap of about 0.55 and 0.65 eV on the density of states of a semiconducting tube having the average diameter of 1.48 and 1.36 nm respectively. However, the

potential window should not be extended to the extent that may cause the electrolyte decomposition especially in the case of aqueous H_2SO_4 electrolyte, which will give rise to redox peaks on the cyclic voltammogram, and it will become difficult to analyze any of the changes occurring on the voltammogram in terms of the electronic density of states. For this reason CV measurement H_2SO_4 in wide potential window was disregarded. Then CV measurement was repeated for sample A with 1.0 M NaI aqueous solution (Figure 3). The dumbbell shape was obtained once again with similar "grip distance" to that shown in Figure 2(a) (approximately 566 mV). This was followed by an abrupt increase in the electrode capacitance.

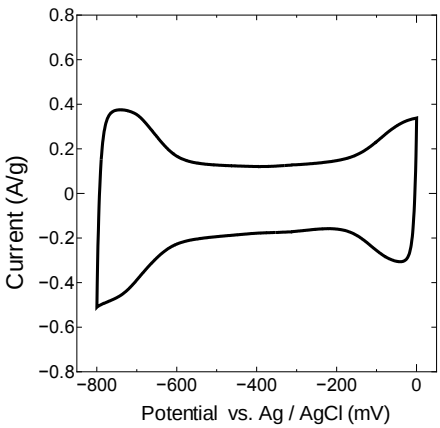

Fig.3 Cyclic Voltammogram of sample (A) SWCNTs in NaI

Thus, we conclude that the cyclic voltammogram reflected the characteristic electronic structure of SWCNTs, as shown in Figure 2. The two samples, both of which exhibit high crystallinity and narrow diameter distribution, show dumbbell-like voltammograms with two different "grip-distance" widths that correlate to the energy band gap of their respective densities of states. Subsequently, two "step-like" humps of higher capacitance values appear. This was apparently caused by the increase in the number of charge carriers supposedly providing additional energy to push the ions inside the decapped tubes, thus increasing the electrode capacitance.

Before we consider the ion adsorption inside the tubes, it is important to observe the region that we will call "the dumbbell grip" in the middle of the voltammograms in Figure 2. In that region the value of electrode capacitance of open-end tubes is similar to that of closed-end tubes. It was also seen from charge-discharge measurements that the specific capacitance per unit surface area for open-end B sample (5.7 μF/ cm^2) is higher than that of open-end A sample (3.6 μF/ cm^2), which is in accordance with other results obtained for nano-scale pore size (<2 nm), [15] and suggests more compact ion packing inside the tubes of sample B due to their smaller size. [35] One possible rationalization for this is the removal of more solvation shells surrounding the ions in the case of sample B with smaller tube diameter than in the case of sample A whose tube diameter is larger. The unfavourable free energy of the removal of solvation shells offers one possible explanation for the observation that open-end tubes for both samples have capacitance value similar to their closed-end counterparts at low applied potential. [(14, 35)] In other words, our observation suggests that; depending on the ion size. the wetting of the electrode pores with the electrolyte ions may or may not take place as a function of the applied potential, which seems to contradict the hypothesis that the electrode pores are completely wetted with the electrolyte even at the potential of zero charge.[35] This also suggests that the ion adsorption at low applied potential is not favourable on the inner surface of the tube due the constrained nature of the surface inside the tubes. However, since the present data do not offer enough insight into the actual ion size and number of solvation shells surrounding the ion in each of the two samples, more detailed theoretical consideration of SWCNT structure is required to obtain an accurate image of the ion adsorption in such system at different applied potentials.

Next, to consider the adsorption inside SWCNTs the "grip" region is disregarded and the focus will be on the "step-like" hump. In this potential range, the capacitance of open-end tubes is higher than that of closed-end tubes. Therefore, ion adsorption seems to occur inside the tubes in the region of the "step-like" hump. Thus, we postulate that variation in the ion adsorption behaviour in the hump region is related to the specific nature of the space inside open-end SWCNTs. H_2SO_4 can be examined in this window without decomposition. Only sample A was considered, given its significantly higher crystallinity and well-defined structure compared to sample B, which is shown by the XRD patterns in Figures S1 and S2. To analyse the ion adsorption behaviour, cyclic voltammetry was performed in several electrolyte solutions at varying scan rates.

First, the cyclic voltammetry measurements were taken in a potential range sufficiently wide to display the complete dumbbell shape (Figure 4). Comparing the cyclic voltammogram of NaCl electrolyte solution to that of NaI solution, it was observed that the two voltammograms exhibit the same shape in the same range of applied potential (−800 – 0 mV) indicating that the dumbbell shape is the result of the fundamental features of the tube rather than the electrochemical environment. Also, we observed a second instance of increase in the capacitance (second hump) at a voltage of approximately 500 mV, which could be assigned to the first van Hove singularity of the (15, 6) metallic tubes.

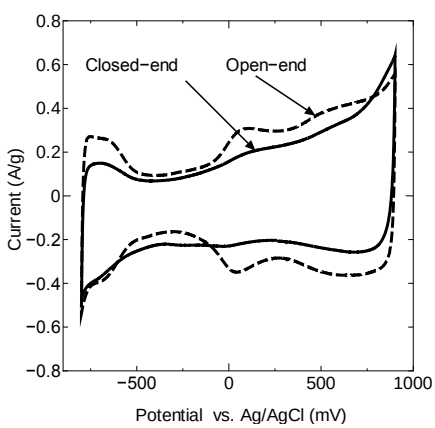

Fig.4 Cyclic Voltammogram of closed- and open-end sample A SWCNTs in NaCl

Neglecting the grip region, a potential between 0 and 800 mV was selected to investigate ion adsorption inside the SWCNTs. Over this range, the capacitance value of open-end tubes may be significantly higher than that of closed-end tubes. In the selected potential range, we performed CV for NaCl (Figure 5) and H_2SO_4 (Figure 6) solutions. Figures 5 and 6 show the effect of decapping on the electrode capacitance; the capacitance of open-end tubes in both electrolytes is higher than that in closed-end tubes. We can postulate that additional ion adsorption was taking place inside decapped tubes in both electrolytes, resulting in additional capacitance. Also, the two electrolytes seem to be different in terms of ion adsorption behaviour inside SWCNTs. While the CV curve for closed-end tubes in both NaCl and H_2SO_4 (Figures 5(a) and 6(a), respectively) maintains a uniform shape despite the increase in the scan rate, the shape of cyclic voltammogram and value of the capacitance in open-end tubes apparently vary depending on the type of the electrolyte. In the case of open-end tubes in NaCl, an increase in the scan rate causes deformation of the CV curve, showing signs of ohmic drop and lower electrode capacitance (Figure 5(b). Such deformation was insignificant for closed-end tubes, and thus the ohmic drop causing the deformation can be primarily attributed to the inner resistance of ion diffusion in the new porous structure introduced by decapping the tubes. With H_2SO_4, it was observed that the behaviour of open-end tubes (Figure 6(b)) was similar to that of closed-end tubes (Figure 6(a)), and showed no deformation in the CV curve despite the increase in the capacitance that clearly indicates that additional ion adsorption was taking place inside open-end tubes.

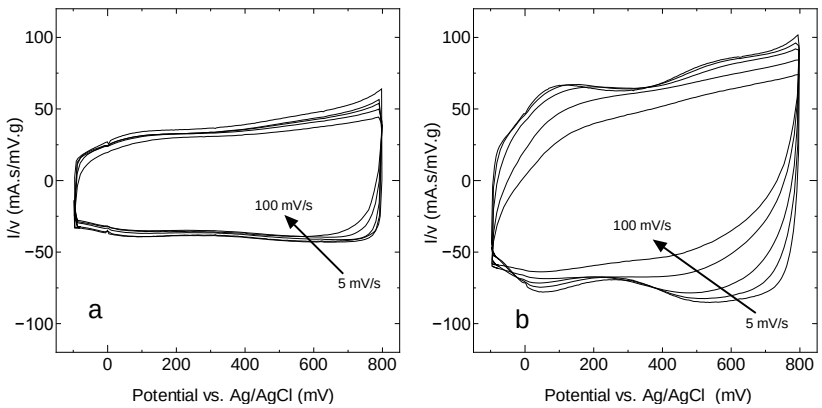

Fig.5 Cyclic Voltammograms depicting current (I) at scan rates (v) of 5, 10, 20, 50, and 100 mV/s. The arrow indicates the direction of increasing the scan rate (a) closed-end and (b) open-end SWCNTs in NaCl

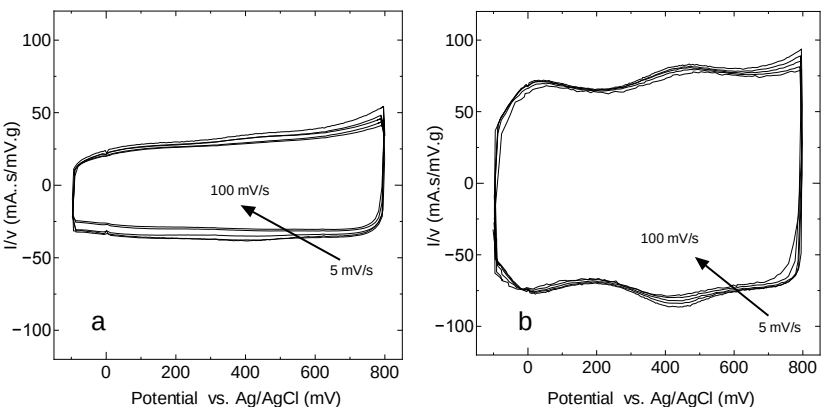

Fig.6 Cyclic Voltammograms depicting current (I) at scan rates (v) of 5, 10, 20, 50, and 100 mV/s. The arrow indicates the direction of increasing the scan rate (a) closed-end and (b) open-end SWCNTs in H_2SO_4

Owing to the entanglement of SWCNTs in the bundle, the ion storage in closed-end tubes possibly occurred on the outer surface of the bundle mat and in the inter-bundle spaces, allowing ions to diffuse easily along the adsorption surface. Storage space with respect to the tube diameter range investigated in this study is sufficiently large not to impose any constraints on ion adsorption and displays the behaviour of a flat electrode. Thus, ohmic drop effect was not observed in closed-end tubes in the two electrolytes.

In the open-end tubes, the additional ion storage space was the tubular channel inside the SWCNT, which provides a constrained diffusion path. The ion diffusion requires sufficient time to proceed down the tubular channel and is likely to become dependent on the type of the ion. In the case of NaCl, the diffusion of Na^+ and Cl^- ions is the result of ion migration. At high scan rates, the pores may not be able to follow the variation in potential as quickly as the outer surface of the bundle.[36] As a result, the time available for the ions to diffuse all the way inside the tubes is insufficient, and the scan is likely to be reversed before full-path penetration is attained. This shorter penetration depth reduces the electrolyte concentration and ionic conductivity and increases the internal resistance down the tubular pore, thus resulting in lower capacitance and a deformed voltammogram as

the scan rate is increased. $TEMABF_4$/PC exhibits similar deformation on the voltammogram with an increase in the scan rate (Figures S7 and S8). This is evident for the closed-end tubes possibly owing to the higher viscosity of propylene carbonate solvent and the lower mobility of $TEMA^+$ and BF_4^-, which are larger in size than Na^+ and Cl^-, especially in their solvated state.

With H_2SO_4, the fact that, at all scan rates investigated, the cyclic voltammograms of both closed-end and open-end do not exhibit any deformation, implies that the adsorption spaces outside and inside the tubes are both easily accessible. Such behaviour might be expected, considering that H_2SO_4 dissociates in water to give protons H^+ with high ionic mobility. The proton mobility occurs as a result of two mechanisms: the hydrodynamic migration of hydronium ion (H_3O^+) and the "proton jump," i.e., the transfer of an H^+ ion from one water molecule to the neighbouring one, along a chain of water molecules. The combined effect of these two mechanisms leads to high mobility and high ionic conductivity.[37] On the other hand, the anion contribution to the observed behaviour in Figure 6 (b) cannot be easily judged. This is caused by the possibility of both HSO_4^- and SO_4^{2-} ions coexisting in the solution with a population that is crucially determined by the number of surrounding water molecules coordinating with the ions.[38] Nevertheless, the reported conductivity of H_2SO_4 is significantly higher (approximately 4 times) than that of NaCl and possibly results in low ohmic drop shown in Figure 6(b).

To quantitatively assess of the change in ohmic drop imposed by the nature of adsorption in the inner tubular structure of SWCNTs, we employed an analytical approach to reproduce the experimental results of the present study. Our approach explains the variation in the shape of the cyclic voltammogram relative to the time required for the ions to diffuse down the pore length at different scan rates. Ions generally require a longer time to travel down the path inside the porous structure of the space inside the tubes when compared with the outer surface of the tube that offers a shorter, straighter diffusion path.

We represent the ion adsorption process with the resistor-capacitor-in-series equivalent circuit. The potential across the resistor is given by Ohm's law, ($E_1 = IR$). Then we define the potential across the capacitor ($E_2 = Q/C$).

We combine both expressions and differentiate them with respect to time to obtain a time dependent expression for the potential across the equivalent circuit:

$$E(t) = RI(t) + Q(t)/C \qquad (1)$$

Where R is the resistance, Q the electric charge, and C the double layer capacitance. The above equation is solved to obtain the current as a function of time:

$$I(t) = Cv\,\{1-(1-I_o/Cv)\exp(-t/RC)\} \qquad (2)$$

Where I_o and I are the electric current at time values (0) and (t), respectively. Then the time is rephrased as (E/ν), where (ν) is the potential scan rate. The following is the final equation that predicts the current through the EDLC:

$$I(E) = Cv\,\{1-(1-I_o/Cv)\exp(-(E-E_o)/vRC)\} \qquad (3)$$

Using equation 3, we have prepared plots of mathematically calculated CV curves under the same applied potential and scan rates used in the experiments. Using a trial and error procedure, we varied the values of both the constants C and R until the values that lead to the closest possible accordance between the experimentally measured and the mathematically calculated data were reached (see Figure 7 for an example of open-end sample in NaCl). The value of R obtained from this trial and error procedure was considered the electrode resistance. The process was performed for each of the different electrode/electrolytes combinations, as seen in Table S2. The results reflect the difference relative to the electrode resistance and its dependence on the type of electrolyte.

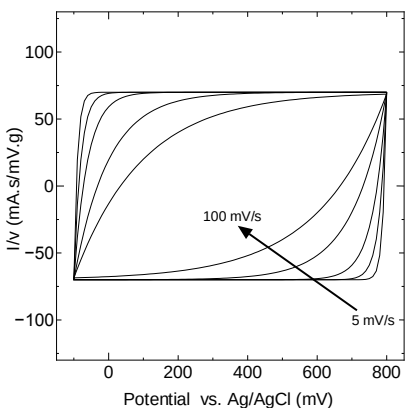

Fig.7 Example for Simulation of CV curve for open-end SWCNT in NaCl at scan rates of 5, 10, 20, 50, and 100 mV/s. The arrow indicates the direction of increasing the scan rate

For H_2SO_4, both closed- and open-end SWCNTs have the same resistance values. On the other hand, the electrode resistance of open-end tubes is three and 1.5 times that of closed-end tubes in NaCl and $TEMABF_4$, respectively.

3. Experimental

Two SWCNT samples of different average diameters denoted as sample A and sample B were used in the present study. The average diameter of sample A was 1.48 nm (Meijo Nano Carbon Co. Ltd., produced by arc discharge), and that of sample B was 1.36 nm (provided by the Faculty of Science, Chiba University, produced by laser ablation). The as-grown samples were purified to remove catalyst impurities. Both samples were heat treated at 300 °C to remove amorphous carbon. The narrow diameter distribution of both samples was confirmed by Raman spectroscopy. The Raman spectra were excited by a 514.5 nm Argon laser and collected using a Raman microscope system equipped with an Acton SP 2300 charge-coupled device (CCD) (Princeton Instruments).

Two types of each sample were prepared: closed-end and open-end. The closed-end SWCNTs were prepared by annealing the purified samples at 1200 °C for 14 h in vacuum.[33] The open-end SWCNTs were prepared by heating the closed-end SWCNTs at 450 °C for 20 min in air.[31] To verify the success of the decapping treatment, nitrogen adsorption/desorption measurements were performed to evaluate the specific surface area of both closed-end

and open-end samples. The measurements were performed at 77 K using a Gemini 2375 (Shimadzu).

Cyclic voltammetry (CV) was conducted using a potentiostat/galvanostat (Hokuto Denko) controlled by a computerized system. A specially designed cell with a conventional three-electrode configuration was used. In this cell, an SWCNT sheet sample and an activated carbon sample on a platinum mesh current collector were used as the working and counter electrodes, respectively. CV was performed using 1.0 M H2SO4, 1.0 M NaCl, and 1.0 M triethylmethylammonium tetrafluoroborate ($TEMABF_4$) in propylene carbonate (PC) as electrolyte solutions. An Ag/Ag^+ reference electrode was used with $TEMABF_4$/PC, and Ag/AgCl was used as the reference electrode for aqueous electrolytes. CV was conducted at scan rates between 5 and 100 mV/s with an argon-filled dry box as the measurement environment for the organic electrolyte. Also, charge-discharge measurement was performed with current densities between 50 and 1000 mA/g.

Conclusions

Ion adsorption on the inner surface of SWCNTs requires higher energy than the outer surface. The constrained size makes this inner surface more sensitive to the nature and size of electrolyte ions. The increase in the number of charge carriers upon doping apparently provides the additional driving force that is required to push the ions inside open-end SWCNTs, leading to sudden increase in the electrode capacitance and resulting in a “step-like” hump on the cyclic voltammogram of SWCNTs when the sample has high crystallinity and narrow diameter distribution. To accurately describe the adsorption behaviour of different ions in different adsorption sites on SWCNTs, it is necessary to expand the array of electrolytes used and address the process of charge transfer resistance on the outer and inner surfaces of the tubes in detail, and the role of the tube diameter combined with the elements mentioned above must be considered to appropriately map the electrochemical behaviour of SWCNTs.

Notes and references

[a] *Department of Materials Science and Engineering, Nagoya Institute of Technology.Gokiso-cho, Showa-ku, Nagoya, Aichi, 466-8555 Japan. Tel: +81-52-735-5221 Fax: +81-52-735-5221*

[*] *Corresponding Author email: kawasaki.shinji@nitech.ac.jp*

† Electronic Supplementary Information (ESI) available: Figure S1, XRD for sample (A) SWCNTs; Figure S2, XRD for sample (B)SWCNTs; Figure S3, Kataura plot; Figure S4, Raman spectra for open-end A and B SWCNTs; Figure S5, Nitrogen adsorption isotherms for A SWCNTs; Figure S6, Nitrogen adsorption isotherms for B SWCNTs; Figure S7, Cyclic Voltammogram for closed-end of sample A SWCNTs in $TEMABF_4$; Figure S8, Cyclic Voltammogram for open-end of sample A SWCNTs in $TEMABF_4$; Table S1, The Brunauer–Emmett–Teller surface area of the SWCNT samples used; Table S2, The total ohmic resistance for both types of SWCNTs.

1 P. Simon, and Y. Gogotsi, *Phil. Trans. R. Soc. A*, 2010, **368**, 3457.
2 R. Kötz, and M. Carlen, *Electrochim. Acta*, 2000, **45**, 2483.
3 L. Eliad, G. Salitra, I. Soffer, and D. Aurbach, *J. Phys. Chem. B*, 2001, **105**, 6880.
4 J. Chmiola, G. Yushin, R. K. Dash, E. N. Hoffman, J. E. Fischer, M. W. Barsoum, and Y. Gogotsi, *Electrochem. Solid-State Lett.*, 2005, **8**, 7, A357.
5 J. Chmiola, G. Yushin, Y. Gogotsi, C. Portet, P. Simon, and P. L. Taberna, *Science*, 2006, **313**, 1760.
6 M. Eikerling and A. A. Kornyshev, E. Lust, *J. Electrochem. Soc.*, 2005, 152, 1, E242.
7 P. Simon and Y. Gogotsi, *Nat. Mat.*, 2008, **7**, 11, 845.
8 C. Portet, G. Yushin, and Y. Gogotsi, *J. Electrochem. Soc.*, 2008, **155**, 7, A531.
9 J. Chmiola, C. Largeot, P. L. Taberna, P. Simon, and Y. Gogotsi, *Angew. Chem. Int. Ed.*, 2008, **47**, 3392.
10 R. Lin, P. L. Taberna, J. Chmiola, D. Guay, Y. Gogotsi, and P. Simon, *J. Electrochem. Soc.*, 2009, **156**, 1, A7.
11 A. Kajdos, A. Kvit, J. Jagillo, and G. Yushin, *J. Am. Chem. Soc.*, 2010, **132**, 10, 3252.
12 C. Largeot, C. Portet, J. Chmiola, P. Taberna, Y. Gogotsi, and P. Simon, *J. Am. Chem. Soc.* 2008, **130**, 2730.
13 S. Kondrat, and A. Kornyshev, *J. Phys.: Condens. Matter*, 2011, **23**, 022201.
14 S. Kondrat, N. Georgi, M. V. Fedorov and A. A. Kornyshev, *Phys. Chem. Chem. Phys.*, 2011,**13**, 11359.
15 J. Huang, B. G. Sumpter, and V. Meunier, *Angew. Chem. Int. Ed.*, 2008, **47**, 520.
16 S. Kondrat, C. R. Perez, V. Presser, Y. Gogotsi and A. A. Kornyshev, *Energy Environ. Sci.*, 2012, **5**, 6474.
17 K. Hata, D. N. Futaba, K. Mizuno, T. Namai, M. Yumura, and S. Iijima, *Science*, 2004, **306**, 1362.
18 T. Hiraoka, A. Izadi-Najafabadi, T. Yamada, D. N. Futaba, S. Yasuda, O. Tanaike, H. Hatori, M. Yumura, S. Iijima, and K. Hata, *Adv. Funct. Mat.*, 2010, **20**, 422.
19 H. Z. Geng, X. B. Zhang, S. H. Mao, A. Kleinhammes, H. Shimoda, Y. Wu, and O. Zhou, *Chem. Phys. Lett.*, 2004, **399**, 109.
20 M. R. Pederson and J. Q. Broughton, *Phys. Rev. Lett.*, 1992, **69**, 18, 2689.
21 K. Urita, Y. Shiga, T. Fujimori, T. Iiyama, Y. Hattori, H. Kanoh, T. Ohba, H. Tanaka, M. Yudasaka, S. Iijima, I. Moriguchi, F. Okino, M. Endo, and K. Kaneko, *J. Am. Chem. Soc.*, 2011, **133**, 10344.
22 Q.X. Liu, C.X. Wang, S.W. Li, J.X. Zhang, and G.W. Yang, *Carbon*, 2004, **42**, 629.
23 O. Kimizuka, O. Tanaike, J. Yamashita, T. Hiraoka, D. N. Futaba, K. Hata, K. Machida, S. Suematsu K. Tamamitsu, S. Saeki, Y. Yamada, and H. Hatori, *Carbon*, 2008, **46**, 1999.
24 Y. Yamada, O. Kimizuka, O. Tanaike, K. Machida, S. Suematsu, K. Saeki, S. Tamamitsu, Y. Yamada, and H. Hatori, Electrochem. *Solid-State Lett.*, 2009, **12**, 3, K14.
25 Y. Yamada, O. Kimizuka, K. Machida, S. Suematsu, K. Tamamitsu, S. Saeki, Y. Yamada, N. Yoshizawa, O. Tanaike, J. Yamashita, F. Don, K. Hata, and H. Hatori, *Energy Fuels*, 2010, **24**, 3373.
26 A. Izadi-Najafabadi, T. Yamada, D. N. Futaba, H. Hatori, S. Iijima, and K. Hata, *Electrochem. Commun.*, 2010, **12**, 1678.
27 D. N. Futaba, K. Hata, T. Yamada, T. Hiraoka, Y. Hayamizu, Y. Kakudate, O. Tanaike, H. Hatori, M. Yumura, and S. Iijima, *Nat. Mater.*, 2006, **5**, 987.
28 Y. Yamada, T. Tanaka, K. Machida, S. Suematsu, K. Tamamitsu, H. Kataura, and H. Hatori, *Carbon*, 2012, **50**, 1422.
29 P.W. Ruch, R. Kötz, and A. Wokaun, *Electrochim. Acta*, 2009, **54**, 4451.
30 P.W. Ruch, L. J. Hardwick, M. Hahn, A. Foelske, R. Kötz, and A. Wokaun, *Carbon*, 2009, **47**, 38.
31 A. Al-zubaidi, T. Inoue, T. Matsushita, Y. Ishii, T. Hashimoto, and S. Kawasaki, *J. Phys. Chem. C*, 2012, **116**, 14, 7681.
32 M.S. Dresselhaus, G. Dresselhaus, R. Saito, and A. Jorio, *Phys. Rep.*, 2005, **409**, 47.
33 A.G. Rinzler, J. Liu, H. Dai, P. Nikolaev, C. B. Huffman, F. J. Rodriguez-Macias, P. J. Boul, A. H. Lu, D. Heymann, D. T. Colbert, R. S. Lee, J. E. Fischer, A. M. Rao, P. C. Eklund, and R. E. Smalley, *Appl. Phys. A*, 1998, **67**, 29.
34 1D DOS (van Hove singularity), Shigeo MARUYAMA's Fullerene and Carbon Nanotube Site; University of Tokyo. http://www.photon.t.u-tokyo.ac.jp/~maruyama/kataura/kataura.pdf.
35 C. Merlet, B. Rotenberg, P. A. Madden, P. L. Taberna, P. Simon, Y. Gogotsi and M. Salanne, *Nat. Mater.* 2012, **11**, 306.
36 R. De Levie, *Electrochim. Acta*, 1963, **8**, 751.

37 T. Erdey-Grúz, in *Transport Phenomena in Aqueous solutions*, Akademiai Kaido: Budapest and Adam Higler, The Institute of Physics: Bristol, England, 1974; pp. 278-284.
38 S. Sugawara, T. Yoshikawa, and T. Takayanagi, *J. Phys. Chem. A*, 2011, **115**, 11486.